Correlations Between Sea-Surface Salinity Tendencies and Freshwater Fluxes in the Pacific Ocean

Zhen Li and David Adamec

Abstract

Temporal changes in sea-surface salinity (SSS) from 21 years of a high resolution model integration of the Pacific Ocean are correlated with the freshwater flux that was used to force the integration. The correlations are calculated on a 1°x1° grid, and on a monthly scale to assess the possibility of deducing evaporation minus precipitation (E-P) fields from the salinity measurements to be taken by the upcoming Aquarius/SAC-D mission. Correlations between the monthly mean E-P fields and monthly mean SSS temporal tendencies are mainly zonally-oriented, and are highest where the local precipitation is relatively high. Nonseasonal (deviations from the monthly mean) correlations are highest along mid-latitude storm tracks and are relatively small in the tropics. The response of the model's surface salinity to surface forcing is very complex, and retrievals of freshwater fluxes from SSS measurements alone will require consideration of other processes, including horizontal advection and vertical mixing, rather than a simple balance between the two.

POPULAR SUMMARY

Title: Correlations Between Sea-Surface Salinity Tendencies and Freshwater Fluxes in the Pacific Ocean

Authors: Z. Li and D. Adamec/614.2

Summary: One of the goals of NASA's new mission to measure the global sea-surface salinity will be to determine how much of the temporal changes in sea-surface salinity is directly due to the additions and subtractions of fresh water to and from the ocean. Addition of freshwater is accomplished through precipitation, and subtraction through evaporation. Whereas precipitation can be measured from satellites, there is no current available technology for a direct measurement of evaporation from space. It is hoped that salinity changes would provide a useful proxy for these important freshwater fluxes, that among other things, determines the long climate-scale flows in the ocean known as the thermohaline circulation and the global ocean conveyor belt.

A sophisticated and realistic ocean computer model is forced with prescribed evaporation and precipitation fields. The computer-generated salinity fields are then used to determine how much of the changes in salinity are due to that forcing and how much of the changes are due to other processes such as movement of salt by ocean currents, or stirring of the surface waters by the wind. It turns out that the ocean computer model's response to the prescribed inputs is very complex, and simple balances between salinity changes and precipitation and evaporation fields are the exception as opposed to the rule. Retrieving freshwater additions and subtractions to the ocean will require careful consideration of the ocean currents, and how easily surface waters are stirred by the atmosphere.

Correlations Between Sea-Surface Salinity Tendencies and Freshwater Fluxes in the Pacific Ocean

Zhen Li

Science Applications International Corporation, Beltsville, Maryland, USA

David Adamec

Oceans Sciences Branch, NASA Goddard Space Flight Center, Greenbelt, Maryland, USA.

D. Adamec, Oceans Sciences Branch, Code 614.2, NASA Goddard Space Flight Center, Greenbelt, MD 20771, USA

Z. Li, Global Modeling and Assimilation Office (GMAO), Code 610.1, NASA Goddard Space Flight Center, Greenbelt, MD 20771, USA. (zhen.li@gsfc.nasa.gov)

Temporal changes in sea-surface salinity (SSS) from 21 years of a high resolution model integration of the Pacific Ocean are correlated with the freshwater flux used to force the integration. The correlations are calculated on a 1^ox1^o grid, and on a monthly scale to assess the possibility of deducing evaporation minus precipitation (E-P) fields from the salinity measurements to be taken by the upcoming Aquarius/SAC-D mission. Correlations between the monthly mean E-P fields and monthly mean SSS temporal tendencies are mainly zonally-oriented, and are highest where the local precipitation is relatively high. Nonseasonal (deviations from the monthly mean) correlations are highest along mid-latitude storm tracks and are relatively small in the tropics. The response of the model's surface salinity to surface forcing is very complex, and retrievals of freshwater fluxes from SSS measurements will require consideration of other processes, including horizontal advection and vertical mixing.

1. Introduction

The science goals of the joint United States-Argentina sea-surface salinity (SSS) observing mission, Aquarius/SAC-D, are to understand the role of salinity variations in climatic processes, and to understand how salinity variations influence the ocean's general circulation (Lagerloef *et al.*, 2002; Koblinsky *et al.*, 2003). To attain these goals, it is envisioned that accurate maps of the flux of freshwater between the ocean and atmosphere, usually represented as the difference between evaporation and precipitation (E-P), will be derivable from the temporal changes in SSS observed by Aquarius/SAC-D.

The mission science requirement of Aquarius/SAC-D is to deliver measurements of the global SSS at a spatial resolution of 100 km every month. The nominal accuracy of those SSS measurements is to be no worse than 0.2 - 0.3 practical salinity units (psu). The approximate 30-day temporal resolution is too long to capture fast ocean processes such as entrainment and detrainment in the mixed layer, and possibly too long for determining the effects of horizontal advection when the advecting velocities exceed 4cm/s ($\sim$ 100km/30days). Thus, obtaining reliable E-P estimates from surface salinity changes will rely on the effects of fast, i.e., faster than 30 days (e.g., tropical instability waves or wind stirring), ocean processes acting randomly that do not introduce their own relatively large time-integrated tendencies in the SSS.

Delcroix *et al.* (1996) examine the relationship between temporal changes in the observed SSS provided by ships of opportunity and rainfall estimates derived from satellite outgoing longwave radiation, and find a good correspondence between the two in areas with the heaviest precipitation, i.e., the Intertropical and South Pacific convergence zones

(ITCZ and SPCZ). That study averaged data into 10^o zonal by 2.5^o meridional boxes and temporally smoothed the monthly input data. Though not formally calculated, the Delcroix *et al.* study estimates the effect of evaporation would be 30-50% of precipitation changes in the convergence zones, and the effect of advection is responsible for 25% of the local salinity balance near strong currents.

Wijffels (2001) compares 13 different climatological estimates of E-P and finds that differences between products can have a global standard deviation as large as 250mm/yr, and regional differences as large as 500mm/yr. The largest deviations occur predominantly over the tropics and the mid-latitude storm tracks. The deviations between the E-P estimates in that study are mainly due to differing estimates of precipitation over the ocean. The estimates of evaporation, a derived quantity, vary much less than precipitation estimates. The Wijffels study clearly identifies a need for consistent estimates of E-P, even for an annual mean temporal scale.

In this study, a state-of-the-art numerical model is used to simulate variability in the Pacific Ocean. Model surface salinities from a 21-year (1984-2004) period are used to investigate the viability of deriving E-P fields from surface salinity at temporal and spatial resolutions commensurate with Aquarius/SAC-D. The viability is determined by calculating the correlation coefficient between the local temporal changes in the upper most layer salinity and the E-P fields used to force the model. Results for both the seasonal and nonseasonal correlations are presented.

2. Model Setup

The ocean integration utilizes the Modular Ocean Model (MOM) version 4.0 (Griffies *et al.*, 2005). The domain extends 45°S to 50°N and 120°E to 70°W. For simplicity, all lateral boundaries are closed, even though the exchange of salt that occurs in reality between the Indian and Pacific oceans may be locally relevant and affects conclusions of this study there. The horizontal resolution is $1/4^o$, and the model has 43 vertical levels. The vertical resolution is 10 m in the upper 220m, and increases to a maximum of ~500m in the deepest ocean. Bottom topography derives from Smith and Sandwell's (1997) 2.5′ product. The minimum water depth is 100m.

The model initializes with the Levitus 1998 (Levitus *et al.*, 1998) annual mean climatology of temperature and salinity and spins-up for 30 years forced by the NCEP-STR air-sea flux climatology (Doney *et al.*, 1998). The integration then runs for 41 years (1964-2004) using monthly average wind forcing, surface heat and freshwater fluxes from the NCEP/NCAR Reanalysis 1 Data (Kalnay *et al.*, 1996). To avoid possible transient effects after switching to NCEP/NCAR monthly forcing, only model output from last 21 years (1984-2004) of the integration is used in this investigation. The integration uses the standard default settings for mixing parameters (Griffies et al., 2005), including a KPP option for the surface mixed layer parameterization. To avoid drift in the model climatology, a tendency based on the difference between the modeled and observed monthly mean salinity and temperature fields is included. The model surface temperature is relaxed to monthly mean climatology with a 30-day^{-1} damping scale. The surface salinity employs a

weaker 240-day^{-1} damping scale that allows for realistic variability at annual and longer time scales.

3. Forced Surface Layer Salinity Variability

The simulated SSS at the model's 1/4^{o}x1/4^o resolution is averaged to a 1^{o}x1^o grid to match the nominal Aquarius/SAC-D resolution. Evaporation is computed from the latent heat flux data from the NCEP/NCAR reanalysis. Evaporation and precipitation fields are interpolated from their original 1.875^o x 1.9047^o resolution to the coincident 1^{o}x1^o SSS grid.

Two calculations of correlations are presented. The first calculation uses monthly mean values for input, and those inputs and correlations are referred to here as "seasonal". The second correlation uses deviations from monthly mean values and is referred here to as "nonseasonal". For seasonal correlations, values above 0.53 are significant at the 95% confidence level, and for nonseasonal correlations, values above 0.125 are significant at the 95% level.

The standard deviation of seasonal E-P (Figure 1a) has variability that is mainly zonally-oriented. The largest standard deviations occur off the west coast of Central America where precipitation has a marked summertime peak due to convection. This area is also a genesis area for hurricane formation in the east Pacific. There are local maxima in the standard deviations at about 18^o latitude in each hemisphere extending out from the western boundary. Off the east coast of Australia, the larger standard deviations are due to large values of summertime precipitation and activity associated with the SPCZ. Near the Philippines, the larger standard deviations are more associated with the

seasonal meridional migration of a local maximum in precipitation. East of the dateline, there are local maxima at about 5^o latitude associated with precipitation along a northern and southern branch of the ITCZ. There are also local maxima in the North Pacific along the winter time storm track. The equator and warm pool are areas of low seasonal variability.

The nonseasonal E-P standard deviations (Figure 1b) have maximum variability that is located almost entirely in the tropics west of 160°W. Variability associated with El Nino Southern Oscillation (ENSO) events is responsible for the larger standard deviations in the warm pool. The effects of ENSO reach into the SPCZ and the high variability of precipitation area off the east coast of the Philippines. The warm and cold sea surface temperatures caused by ENSO in the east Pacific affect the local convective activity and hurricane generation off the west coast of Panama, and South America, and that variability is also evident in the non-seasonal standard deviations of E-P.

The standard deviations of the seasonal SSS temporal tendencies (Figure 1c) are mainly zonally oriented as were the seasonal standard deviations in E-P. The largest values are in the eastern equatorial Pacific and near the Korean peninsula that is a natural response to strong E-P forcing from local monsoonal variability. Curiously, this area was not an area of relatively large E-P forcing. The nearby Kuroshio plays an important role for SSS in this area. The nonseasonal standard deviations (Figure 1d) are of larger spatial scale than the seasonal variability. The largest standard deviations are in the eastern and western tropics and are related to ENSO variability. The minimum in the tropics near 150°W is consistent with the area being a pivot point of the normal see saw pattern of variability

in the eastern and western tropical Pacific during an ENSO event. The maximum in the western tropical Pacific is consistent with model calculations performed by Wang and Chao (2004) who showed a maximum in interannual variability of SSS there with RMS values approaching 0.5 psu.

The correlations between the seasonal SSS temporal tendencies and seasonal E-P (Figure 2a) are, not surprisingly, zonally-oriented as were the seasonal signals of the individual fields of standard deviations. What is surprising is that some of the correlations are negative indicating processes that lead, for example, to surface water becoming more saline during periods of less evaporation and more precipitation. It is much easier to comprehend and justify positive correlations when considering the local effect of E-P on salinity tendencies.

In areas of greater seasonal variability of E-P, specifically off the Central American coast, and near 18^o latitude in the western Pacific, the seasonal correlations are strongly positive. These correlations are consistent with the Delcroix *et al.* (1996) study who show consistency on large spatial scales between areas of higher precipitation and negative salinity tendencies. Here, the correlations are also strongly positive along the northern and southern branches of the ITCZ, and along the southern edge of the wintertime Pacific storm track, again in areas of higher precipitation. The southern edge of the storm track is an area of greater precipitation as the synoptic systems are able to tap into moisture provide by the subtropical jet. This explanation provides a rationalization of why the highest correlations are south of the high E-P variability, but does not explain why higher E-P variability is located further to the north. More detailed analyses that involve the

distribution of evaporation associated with the storm track, salinity changes brought about by the Ekman upwelling induced along the storm track and horizontal advective processes need to be accounted for in order to provide a full explanation, and is out of the scope of the present study.

As noted above, there are areas where the seasonal correlation between E-P and salinity tendency is negative. In particular, an area along the equator in the eastern Pacific has a very strong negative correlation. This area upwells strongly due to the divergent winds. An investigation of precipitation events in this region revealed those events were also accompanied by stronger surface winds that force increased upwelling. For this region, the freshening of the surface water by the precipitation is masked by an increased upwelling, which tends to bring higher salinity water from below. Note that the equatorial eastern Pacific has shallow mixed layers, and is more susceptible to wind forcing and stirring that brings higher saline waters to the surface. Increased upwelling in areas of shallow mixed layers is a likely explanation for the negative correlations in the areas in the vicinity of the cold tongue, off the coast of Baja, and the zonal strip north of the ITCZ where mixed layers are shallow. Definitive answers to any area's correlation would require a more detailed analysis of the local salt balances.

The correlations between nonseasonal SSS temporal tendencies and E-P (Figure 2b) are relatively small between the 20^o latitude circles, and they are particularly low along the equator. Like the SSS temporal tendencies variability, the scales of low and high correlations are larger spatial scale than the seasonal correlations. The highest correlations occur in the mid-latitudes along the wintertime storm tracks for both hemispheres.

The effect of precipitation alone on surface salinity changes is also considered. The correlation between precipitation alone and salinity tendencies (not shown here) closely resembles the correlations with E-P over most areas of the Pacific Ocean for both the seasonal and nonseasonal signals. The most significant deviation occurs in the seasonal correlations off the east coast of Japan south of the Kuroshio Extension. This area is the location where cold air outbreaks from the Asian continent first encounters the warmer subtropical waters south of the Kuroshio front. It is an area of large evaporation and largest latent heat fluxes in the Pacific. Except for this location where the correlations are lower, most of the correlations are very similar to the correlations calculated using E-P.

There is consistency between the results of this study and the study by Delcroix *et al.* (1996). Both studies show a high positive correlation between SSS temporal tendencies and E-P in areas of relatively larger rainfall. The difference between the two studies is that the Delcroix *et al.* (1996) study emphasizes larger spatial scales by working with monthly data averaged to 10°x 2.5° boxes, and then looking for similarity from the two leading modes of an empirical orthogonal function EOF decomposition. This study also shows relatively strong positive correlations in areas of largest precipitation even though the calculations are performed with the finer, 1° x 1°, resolution. However, this study reveals finer scale correlation structure with a strong zonal orientation of SSS temporal tendencies and E-P correlations that includes areas where the correlations are negative, particularly in the seasonal signal. This study indicates that extreme care needs to be taken to infer E-P from SSS temporal tendencies away from areas of strongest precipitation.

Finally, because only a 4 cm/s advecting velocity is required to move properties across a 1^o grid box, the role of horizontal advection of SSS tendencies is considered. The seasonal correlations between the salinity temporal tendencies and horizontal advection (Figure 3a) have a similar zonally oriented structure to the E-P calculations. Of note here, the correlations are particularly strong in the tropics west of 160°W and in the subtropical North Pacific. In other areas, the correlation spatial scale is shorter. The nonseasonal correlations (Figure 3b) are more strongly correlated than are the correlations with E-P in most areas. Of particular interest is a local maximum in the area on the equator between 165°E and 160°W. This local maximum is consistent with a study by Delcroix and Picaut (1998) who find surface salinity advection by anomalous zonal, equatorial currents to be the dominant mechanism for surface salinity variations during stronger ENSO events. The stronger nonseasonal correlations in most areas indicate that horizontal advection may somehow need to be estimated for accurate E-P determination from Aquarius/SAC-D measurements for accurate representation of these longer time scales.

4. Summary and Conclusions

The possibility of determining E-P fields from temporal changes in sea-surface salinity is examined using a state-of-the-art numerical model of the Pacific Ocean. The model is integrated with 0.25^o horizontal resolution but the viability of obtaining E-P fields is studied using horizontal and spatial sampling commensurate with the upcoming Aquarius/SAC-D mission. For seasonal variability, the patterns of the correlations between E-P and SSS temporal tendencies tend to be zonally-oriented and are highest where the local precipitation is also relatively high. The result is consistent with a study by Delcroix *et al.*

(1996) who show this to be the case for large horizontal scales in the tropical Pacific. This numerical study not only shows the same conclusion for shorter spatial scales, but it also shows that the areas between local precipitation maxima have low correlations, and sometimes those correlations may be negative if mixed-layers are shallow and winds induce vertical mixing or upwelling. For the nonseasonal signal, the correlations are highest in the mid-latitudes with relatively smaller correlations in the tropics.

Because Aquarius/SAC-D will return monthly SSS values, the role of horizontal advection's driving SSS temporal tendencies was investigated using a similar correlation analysis. The seasonal correlations have a similar zonal orientation to the E-P correlations, but the advection correlations in the Eastern tropical Pacific are higher than the E-P correlations there. The nonseasonal correlations with horizontal advection are relatively higher than all other correlations calculated. The nonseasonal advective correlations include an area on the equator between 165°E and 160°W where Delcroix and Picaut (1998) determine that horizontal advection is the dominant mechanism for driving salinity variability during ENSO events.

Although inferring E-P from local changes in surface salinity may not be easily attained globally, the high correlation between E-P and salinity changes in areas of high precipitation is encouraging. However, estimating E-P in only those areas would require prior knowledge of the P field itself. Further studies that center on dividing the spatial regime along levels of precipitation would seem a next logical step. Also, careful analysis of the entire salinity balance would be necessary for assessing the reliability of E-P estimates derived from sampling such as will be delivered by the Aquarius/SAC-D mission.

Acknowledgments. This research was sponsored by NASA's Science Mission and NASA's Physical Oceanography Program.

References

Delcroix, T., C. Hénin, V. Porte, and P. Arkin (1996), Precipitation and sea-surface salinity in the tropical Pacific Ocean, *Deep Sea Res., 43*, 1123–1141.

Delcroix, T., and J. Picaut (1998), Zonal displacement of the western equatorial Pacific "fresh pool", *J. Geophys. Res., 103* (C1), 1087–1098.

Doney, S. C., W. G. Large, and F. O. Bryan (1998), Surface ocean fluxes and water-mass transformation rates in the coupled NCAR Climate System Model, *J. Climate, 11,* 1422–1443.

Griffies, S. M., *et al.* (2005), Formulation of an ocean model for global climate simulations, *Ocean Science, 1*, 45-79.

Kalnay, E., *et al.* (1996), The NCEP/NCAR 40-year reanalysis project, *Bull. Amer. Meteor. Soc., 77*, 437–470.

Koblinsky, C. J., *et al.* (2003), Sea surface salinity from space: Science goals and measurement approach, *Radio Science, 38*(4), 8064, doi:10.1029/2001RS002584.

Lagerloef, G. S. E. (2002), Introduction to the special section: The role of surface salinity on upper ocean dynamics, air-sea interaction and climate, *J. Geophys. Res., 107*(C12), 8000, doi:10.1029/2002JC001669.

Levitus, S., T. P. Boyer, M. E. Conkright, T. O'Brien, J. Antonov, C. Stephens, L. Stathoplos, D. Johnson, and R. Gelfeld (1998), *NOAA Atlas NESDIS 18, World Ocean Database 1998*, vol. 1, *Introduction*, 346 pp., U.S. Gov. Printing Office, Wash., D.C.

Smith, W. and D. Sandwell (1997), Global seafloor topography from satellite altimetry and ship depth soundings, *Science, 277*, 1956–1962.

Wang, X. and Y. Chao (2004), Simulated Sea Surface Salinity variability in the tropical Pacific, *Geophys. Res. Lett., 31*, L02302, doi:10.1029/2003GL018146.

Wijffels, S. E. (2001), Ocean transport of fresh water, in *Ocean Circulation and Climate (observing and Modeling the Global Ocean)*, edited by G. Siedler, J. Church and J. Gould, pp. 475–488, Academic Press, London, UK.

LIST OF FIGURES

Figure 1. Standard deviations of (a) seasonal E-P (mm/month), (b) nonseasonal E-P (mm/month), (c) seasonal $\partial S/\partial t$ (psu/month) and (d) nonseasonal $\partial S/\partial t$ (psu/month). For this calculation, one month is equal to 30 days.

Figure 2. (a) Correlations between seasonal $\partial S/\partial t$ and seasonal E-P, and (b) correlations between nonseasonal $\partial S/\partial t$ and nonseasonal E-P. For seasonal correlations, values above 0.53 are significant at the 95% confidence level, and for nonseasonal correlations, values above 0.125 are significant at the 95% level.

Figure 3. (a) Correlations between mean seasonal $\partial S/\partial t$ and mean seasonal surface salinity advection, $-(uS_x + vS_y)$, and (b) correlations between nonseasonal $\partial S/\partial t$ and nonseasonal surface salinity advection, $-(uS_x + vS_y)$. For seasonal correlations, values above 0.53 are significant at the 95% confidence level, and for nonseasonal correlations, values above 0.125 are significant at the 95% level.

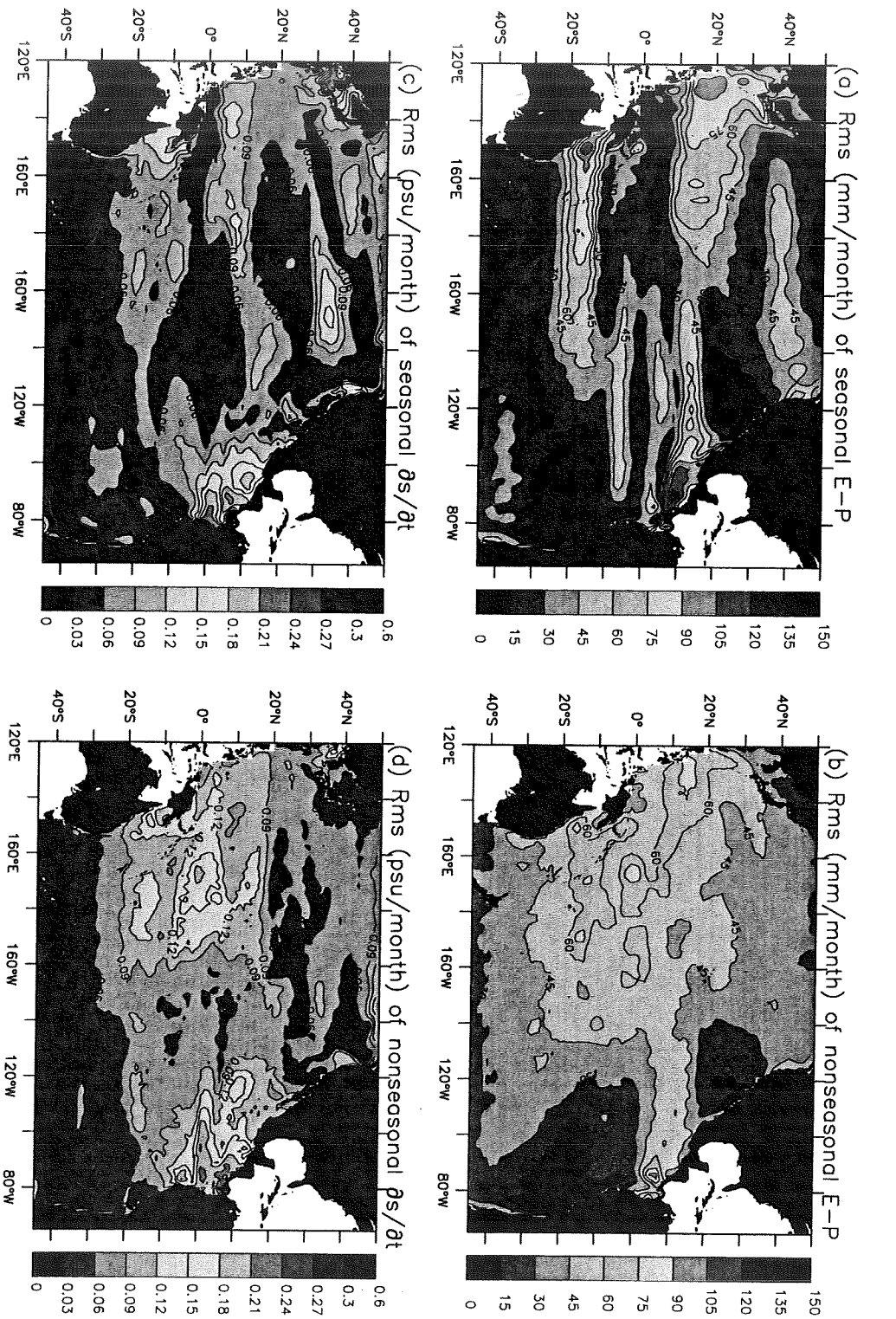

Figure 1. Standard deviations of (a) seasonal E-P (mm/month), (b) nonseasonal E-P (mm/month), (c) seasonal $\partial S/\partial t$ (psu/month) and (d) nonseasonal $\partial S/\partial t$ (psu/month). For this calculation, one month is equal to 30 days.

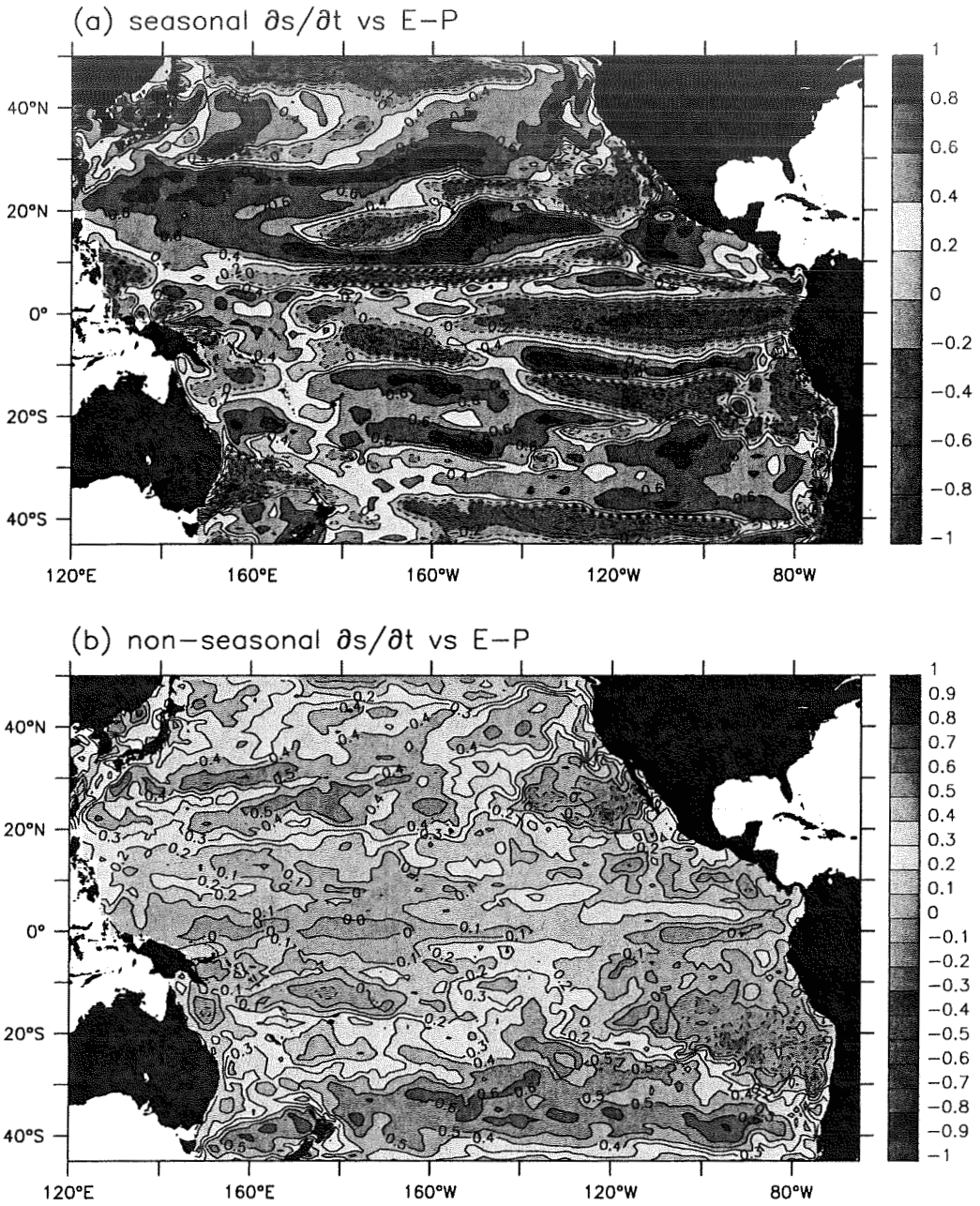

Figure 2. (a) Correlations between seasonal $\partial S/\partial t$ and seasonal E-P, and (b) correlations between nonseasonal $\partial S/\partial t$ and nonseasonal E-P. For seasonal correlations, values above 0.53 are significant at the 95% confidence level, and for nonseasonal correlations, values above 0.125 are significant at the 95% level.

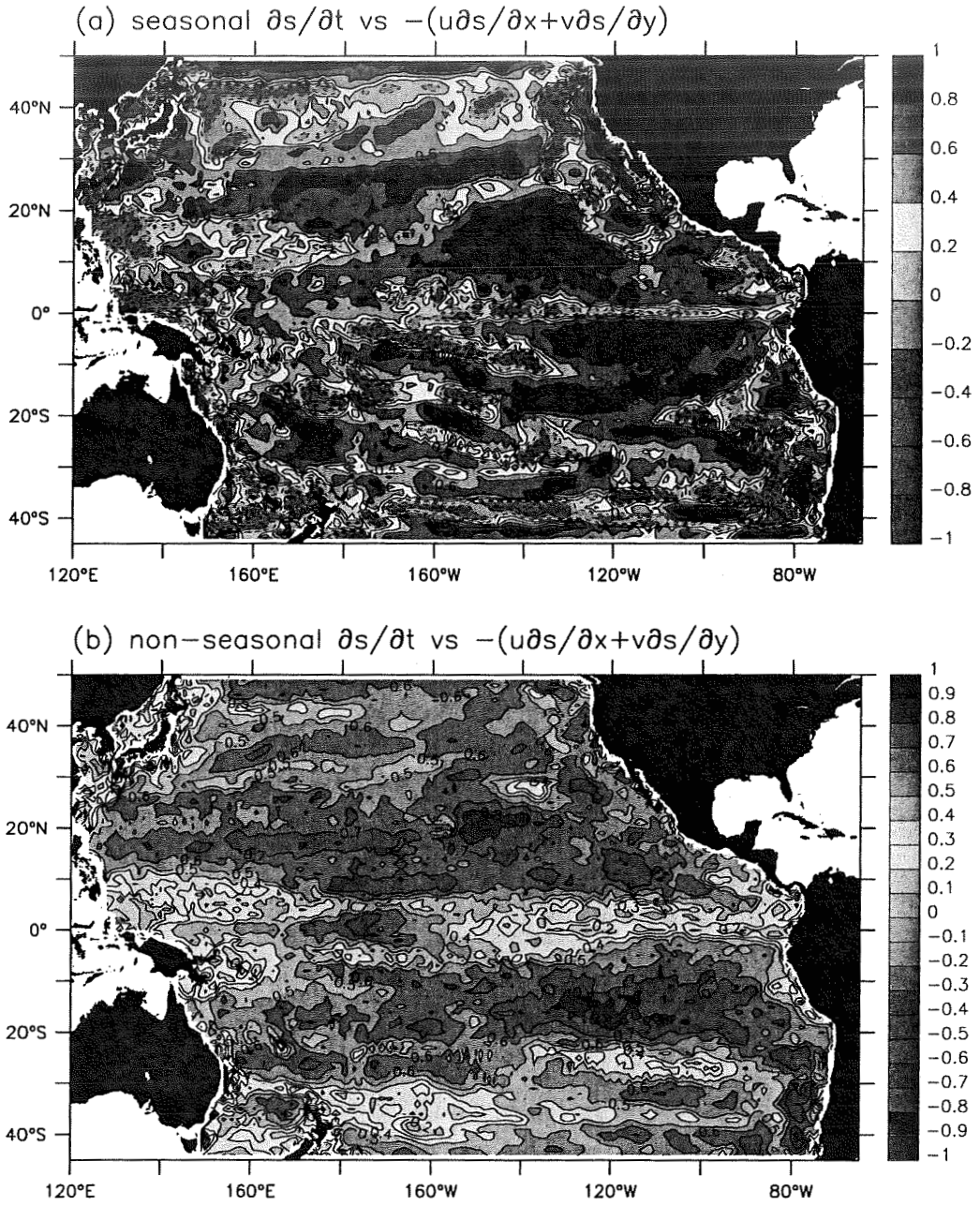

Figure 3. (a) Correlations between seasonal $\partial S/\partial t$ and seasonal surface salinity advection, $-(uS_x + vS_y)$, and (b) correlations between nonseasonal $\partial S/\partial t$ and nonseasonal surface salinity advection, $-(uS_x + vS_y)$. For seasonal correlations, values above 0.53 are significant at the 95% confidence level, and for nonseasonal correlations, values above 0.125 are significant at the 95% level.